European Polymer Journal 196 (2023) 112228

Contents lists available at ScienceDirect

European Polymer Journal

journal homepage: www.elsevier.com/locate/europolj

Polymer stabilized, phenytoin-loaded nanomicelles as promising nanocarriers: *In silico* and *in vitro* evaluations

Nafiseh Jirofti [a,b], Mahdiye Poorsargol [c], Farkhonde Sarhaddi [d,e], Afsaneh Jahani [a,f], Jamileh Kadkhoda [g], Fatemeh Kalalinia [b,h,*], Abbas Rahdar [i,*], Adriana Cambón [j], Pablo Taboada [j,*]

[a] Orthopedic Research Center, Department of Orthopedic Surgery, Mashhad University of Medical Sciences, Mashhad, Iran
[b] Biotechnology Research Center, Pharmaceutical Technology Institute, Mashhad University of Medical Sciences, Mashhad, Iran
[c] Department of Chemistry, University of Zabol, Zabol 98613-35856, Iran
[d] Department of Pathology, School of Medicine, Zahedan University of Medical Sciences, Zahedan, Iran
[e] Department of Pathology, School of Medicine, Iran University of Medical Sciences, Tehran, Iran
[f] Department of Biomedical Engineering, Faculty of New Sciences and Technologies, Semnan University, Semnan, Iran
[g] Department of Medicinal Chemistry, Faculty of Pharmacy, Tabriz University of Medical Sciences, Tabriz, Iran
[h] Departments of Pharmaceutical Biotechnology, School of Pharmacy, Mashhad University of Medical Sciences, Mashhad, Iran
[i] Department of Physics, University of Zabol, Zabol 98613-35856, Iran
[j] Grupo de Física de Coloides y Polímeros, Departamento de Física de Partículas, Facultad de Física-Instituto de Materiales (IMATUS)-Instituto de Investigaciones Sanitarias (IDIS), Campus Vida, Universidad de Santiago de Compostela, 15782 Santiago de Compostela, Spain

ARTICLE INFO

Keywords:
Nanomicelles
Pluronic F127
Lignin, drug delivery
Cytotoxicity
DFT, antimicrobial

ABSTRACT

Many drugs currently used in clinics to treat different diseases show low solubilities in aqueous solutions and must be then administered with the aid of organic solvents within the designed formulations leading to harmful health effects. For such reason, drug delivery using nanocarriers appears as an excellent alternative since it improves the solubilization and controlled release of many different pharmaceuticals, favoring the decrease of the overall administered therapeutic doses and by diminishing the risk of potential associated adverse side effects. Among the different types of nanocarriers, those based on polymeric micelles are an excellent option since the polymer structure and composition may be tuned in order to regulate the characteristics and properties of the resulting nanoassemblies to maximize drug solubilization and release profiles. For this reason, in this paper a drug delivery nanosystem based on oil-in-water polymeric-based microemulsion used to load the anti-epileptic phenytoin drug (PHT) was developed in the oily phase. Two different biocompatible polymers were evaluated to form the nanomicelles and maximize encapsulation efficiencies and colloidal stability: The amphiphilic triblock copolymer Pluronic F127, which poses the ability to cross the blood brain barrier (BBB), and the natural lipophilic lignin, which bears antipathogenic properties. Density functional theory (DFT) calculations were performed with the 6-31G(d) basis set to elucidate the interactions of PHT with F127 and lignin monomers. Simulation data showed that hydrogen bonding (HB) interactions between PHT, F127 and lignin are the predominant force to allow for drug solubilization and stability. Atoms in molecules (AIM) and natural bond orbital (NBO) analyses were performed to evaluate the strength of such HB. and their drug encapsulation efficiency, release profiles, and antibacterial susceptibility were determined. Moreover, the cytotoxicity of the developed nanoformulations together with a morphological examination of PC12 and NIH cells after drug-loaded nanocarrier administration and subsequent uptake were also investigated. In this manner, the obtained nanocarriers were also characterized by dynamic light scattering (DLS) and zeta potential, showing a nanometer size (between ca. 16 and 22 nm) and surface negative charge. PHT loading into F127 and lignin nanomicelles were ca. 96.7 ± 1.5% and 68.2 ± 3.5%, respectively, and the drug release profile kinetics of F127/PHT-loaded nanomicelles was rather slower compared to that of lignin/PHT-loaded ones. On the other hand, *in vitro* cytotoxicity data

* Corresponding authors at: Biotechnology Research Center, Pharmaceutical Technology Institute, Mashhad University of Medical Sciences, Mashhad, Iran (F. Kalalinia). Department of Physics, University of Zabol, Zabol 98613-35856, Iran (A. Rahdar). Grupo de Física de Coloides y Polímeros, Departamento de Física de Partículas, Facultad de Física-Instituto de Materiales (IMATUS)-Instituto de Investigaciones Sanitarias (IDIS), Campus Vida, Universidad de Santiago de Compostela, 15782, Santiago de Compostela, Spain (P. Taboada).

E-mail addresses: kalaliniaf@mums.ac.ir (F. Kalalinia), a.rahdar@uoz.ir (A. Rahdar), pablo.taboada@usc.es (P. Taboada).

https://doi.org/10.1016/j.eurpolymj.2023.112228
Received 4 April 2023; Received in revised form 13 June 2023; Accepted 14 June 2023
Available online 19 June 2023

confirmed the lack of any significant cytotoxicity of PHT-loaded nanomicelles in both NIH/3T3 and PC12 cell lines, but a slightly higher cell viability and well-preserved cell morphology was observed for PC12 cells compared to NIH/3T3 ones. After culturing in chocolate blood agar medium inoculated with F127/PHT-loaded and lignin/ PHT-loaded nanomicelles, pathogenic bacteria did not grow despite confirming certain antimicrobial character of the encapsulated drug. Hence, thanks to their excellent encapsulation and biocompatibility properties, these nanocarriers appear as an excellent option to configure new drug delivery nanocarriers of hydrophobic drugs.

1. Introduction

For several decades, phenytoin (PHT) has been clinically evaluated as an anti-seizure drug since it inhibits motor functions in the cerebral cortex in a highly selective manner. The mechanism of action involves its binding to an inactivated Na^+ channel to prolong neuronal refractoriness [1]. As a sodium channel blocker, the drug can trespass the blood brain barrier (BBB) and allocate into the brain, but also can be accumulated in other parts of the body including kidneys, liver and lungs, thus, leading to potential adverse side effects after its systemic administration as refractory epilepsy, which is still a major clinical challenge [2]. Due to the dose dependent metabolism of PHT and its narrow therapeutic dose range, even small changes in the drug bioavailability can cause major changes in its serum concentration, thus, involving serious clinical concerns. In particular, a low aqueous solubility and susceptibility to crystallize are particular challenges for suitable PHT delivery, thus, critically affecting drug brain bioavailability and/or associated symptoms of chronic pain, amongst other undesirable effects [3].

Nanotechnology has progressed considerably along last twenty years to provide new potential solutions in the biomedical field, especially in drug delivery. Selected nanomaterials may be assembled to configure suitable nanocarriers to allow controlled drug delivery even through biological barriers, then favoring both an enhancement in the therapeutic efficacy of the entrapped drugs and an improvement of the drug chemical stability whilst minimizing potential toxic side effects [4]. At this respect, physiological barriers such as the BBB limit drugś accessibility to their target sites [5]. Drug concentration is also severely limited by efflux transporters. Then, key goals of drug delivery are both to bypass the BBB and overcome efflux transporters. At this respect, different studies have been conducted to analyze the ability of different types of nanocarriers to overcome BBB and then, being potential candidates for successful brain targeting [6,7]. Amongst the different types of tested nanocarriers, microemulsion-based nanoformulations are particularly interesting. Microemulsions (ME) as dispersed systems consist of hydrophilic and lipophilic phases stabilized with surfactants and/or polymers. These nanocarrier systems have been shown to improve the aqueous solubility of lipophilic drugs and have been widely explored as nanovehicles for brain drug delivery with great success [8–10]. In this regard, PHT encapsulated in different microemulsion-based nanovehicles has been administered as an active, encapsulated bioactive compound for increasing its delivery into brain. For example, to promote a positive charge of the ME to favor cell interactions, triacetin was used to disperse the lipophilic compounds into the core, lecithin to form the carrier shell, Tween 80 to stabilize the nanostructure, and chitosan as the coating material. To achieve the smallest particle size and highest drug loading capacity in the nasal-brain channel, chitosan, lecithin, PHT, and the type of surfactant ratios were optimized [9]. Lee *et al.* developed ME-based formulations using a blend of palm, coconut kernel, and soybean oils to load PHT. It was found that an 1:9 oil-to-surfactant ratio facilitated full ME stability upon mixing with Tween 80. However, blending of coconut kernel and soybean oil provided the fastest drug release rate (93%) after 12 h [10]. In another work, Acharya *et al.* designed a PHT-loaded ME with Capmul® MCM as the oily phase and a Labrasol®/Transcutol® mixture as the surfactant/co-surfactant system. These MEs were physically stable during storage for three months without any toxic effects on sheep nasal mucosa. Evaluation in *in vivo* models demonstrated that intranasal ME administration was the most effective route to achieve efficient drug brain uptake in vivo in comparison to intraperitoneal administration, as confirmed by gamma scintigraphy [9]. However, region-specific overexpression of multidrug efflux transporters at the BBB, such as P-glycoprotein (P-gp), might contribute to multidrug resistance (MDR) by reducing target concentrations of antiepileptic drugs and, thus, the development of nanoformulations which can modulate P-gp function as well as facilitating targeted BBB delivery represents a promising strategy for epilepsy intervention.

For such a reason, in this work we develop novel oil-in-water stabilized nanomicelles as a potential nanocarrier for the encapsulation and sustained release of PHT within their oily phase whilst avoiding potential drug crystallization by using a low freezing temperature oil (ethyl butyrate) and offering protection against plasma protein opsonization and degradation, which is one of the factors reducing the therapeutic efficacy free-administered PHT since ca. 90% of the drug is protein-bounded in plasma and cleared out [11]. To build up the micellar-based nanocarriers two different polymers have been studied as stabilizers thank to their structural and complementary therapeutic properties: the FDA-approved linear triblock copolymer Pluronic F127, which is amphiphilic and flexible, and a more complex organic rigid polymer, lignin, which is mainly of hydrophobic nature but have multiple functional groups which may facilitate the binding/interactions of other molecules. In particular, apart from its stabilizing effect in the nanoformulation, F127 copolymer and related triblock copolymers bearing hydrophilic poly(oxyethylene) and more hydrophobic poly(oxypropylene), poly(oxybutylene) and poly(oxystyrene) blocks introduce the potential ability to overcome efflux transporters and, thus, may favor nanoparticles (NPs), for example, to cross the blood brain barrier (BBB) amongst other biological barriers, as reported in some previous works

a)

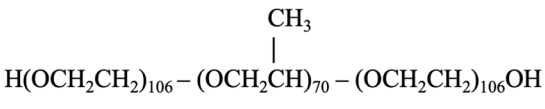

b)

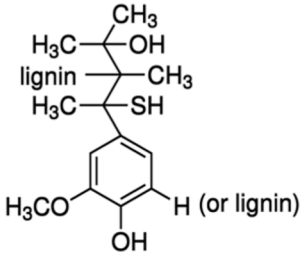

Scheme 1. Molecular formulas of a) F127 and b) lignin.

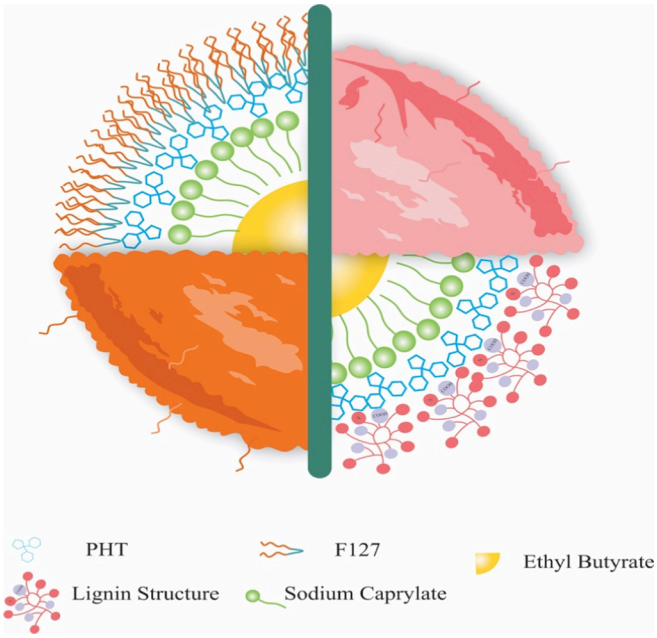

Scheme 2. Schematic representation of PHT-loaded surfactant-based nanomicelles.

[12–15]. Meanwhile, lignin has been proved to possess important anti-pathogenic properties [16,17]. To ensure nanocarrier stability and get key information about the configuration and structure of the micellar-based nanovehicle, binding affinities between both monomeric chains of both F127 and lignin with PHT were estimated by DFT simulations. PHT entrapment efficiency (EE), release profiles, and cytocompatibility of PHT-loaded nanomicelles in neuronal and fibroblasts cell lines were also analyzed for both biocompatible nanotherapeutic systems to characterize the feasibility of the proposed nanovehicles as prospective carriers for drug brain delivery in terms of targeting, pharmacokinetics, biocompatibility and potential gains in therapeutic efficacy.

2. Material and methods

2.1. Materials

Sodium chloride (NaCl), potassium chloride (KCl), potassium dihydrogen phosphate (KH_2PO_4), and sodium phosphate monobasic dihydrate ($NaH_2PO_4{\cdot}2H_2O$) were purchased from Merck (Germany). Sodium caprylate, ethyl butyrate, Pluronic F127 ($EO_{106}PO_{70}EO_{106}$, where EO refers to ethylene oxide and PO to propylene oxide, respectively, and subscripts to the number of monomeric units), lignin (see Scheme 1 for molecular formula) and phenytoin (PHT) were purchased from Sigma Aldrich. For the *in vitro* studies, fetal bovine serum (FBS), Alamar Blue, and Dulbecco's modified Eagle's medium (DMEM) were purchased from Gibco (USA). Dimethyl sulfoxide (DMSO), Roswell Park Memorial Institute (RPMI) 1640 culture medium, trypsin, ethylenediaminetetraacetate (EDTA), penicillin–streptomycin antibiotics, and 3-(4, 5-dimethylthiazol-2-yl)-2, 5-diphenyltetrazolium bromide (MTT) were purchased from Sigma Aldrich. All other materials and solvents used were of analytical grade. All chemicals were used as received without further purification.

2.2. Development of PHT-encapsulated oil-in-water surfactant-based nanomicelles

PHT-loaded oil-in-water surfactant-based biocompatible nanomicelles were developed from dissolving PHT in 1% (w/w) solutions of ethyl butyrate oil by dissolving an amount of fatty acid sodium caprylate (SC, 0.09 g) and F127 (0.008 g) or lignin (0.005 g) phosphate-buffered saline (PBS at pH 7.4) under vigorous stirring at a fixed ethyl butyrate-to-surfactant molar ratio [18] and final total volume of 10 mL. The excess of free PHT was eliminated by dialysis for 24 h. The structure and components of the synthesized PHT-loaded nanomicelles are depicted in Scheme 2.

2.3. Dynamic light scattering (DLS)

To characterize the hydrodynamic size of PHT-loaded based nanomicelles an ALV-5000F static and dynamic light scattering system (ALV GmbH, Germany) was usd. This instrument was equipped with a diode-pumped solid-state laser (2 W, Coherent Innova, USA). The diffusion coefficient of the particles in solution can be obtained from the time variation of light scattering intensity by means of:

$$D = \Gamma/q^2 \tag{1}$$

where Γ the decay rate obtained by fitting a single exponential function to the autocorrelation function of samples and q is the scattering vector:

$$q = \frac{4\pi n}{\lambda}\sin\left(\frac{\theta}{2}\right) \tag{2}$$

The hydrodynamic radii, R_h, of the nanomicelles could be obtained according to the Stokes-Einstein equation [8–9]:

$$\mathrm{R_h} = \frac{k_B T}{6\eta\pi D} \tag{3}$$

where T is the temperature, η is the viscosity of the continuous phase, and K_B is the Boltzmann's constant.

2.4. Drug encapsulation efficiency

The encapsulation efficiency (EE%) of PHT-loaded nanomicelles (F127/PHT-loaded and lignin/PHT-loaded ones) was evaluated by UV–Vis spectroscopy (Shimadzu UV-1700 PharmaSpec, Kyoto, Japan), following the method described by Rahdar *et al.* [19] In this regard, F127/PHT-loaded nanomicelles (and lignin/ PHT-loaded nanomicelles) were centrifuged at 20000 rpm for 60 min. The concentration of PHT in the supernatants was determined by absorbance at 254 nm. Finally, the PHT concentration was calculated by a standard calibration curve, and the EE% calculated using the following equation:

$$\text{Drug loading (DL\%)} = \frac{([\mathrm{PTX}]_{encapsulated})}{[\mathrm{PTX}]_{encapsulated} + [nanocapsules]} \times 100 \tag{4}$$

2.5. Drug release

PHT release profiles for free PHT and PHT-loaded nanomicelles (F127/PHT-loaded and lignin/ PHT-loaded ones) was determined by dialysis experiments using a 10 kDa cut-off dialysis membranes. Accordingly, 1 mL (2 mg/mL) of free PHT in PBS:ethanol 50:50 aqueous mixture and PHT-loaded nanomicelles (F127/PHT-loaded and lignin/ PHT-loaded nanomicelles) in PBS was poured into 10 kDa dialysis membranes. The dialysis bags were immersed in 50 mL of PBS (pH 7.4) and incubated in a shaker incubator at 37 °C (90 rpm). At different time points, 100 μL of the sample solution were transferred to a test tube and replaced with 100 μL of fresh PBS solution. The concentration of released PHT was assessed by UV spectrophotometry (Shimadzu UV-1700 PharmaSpec, Kyoto, Japan) at 254 nm. Finally, the concentration of PHT at each time point was evaluated by a standard calibration curve and expressed as the percent of cumulative drug released.

2.6. Cytotoxicity evaluation

Cytotoxicity of free PHT, unloaded and PHT-loaded nanomicelles

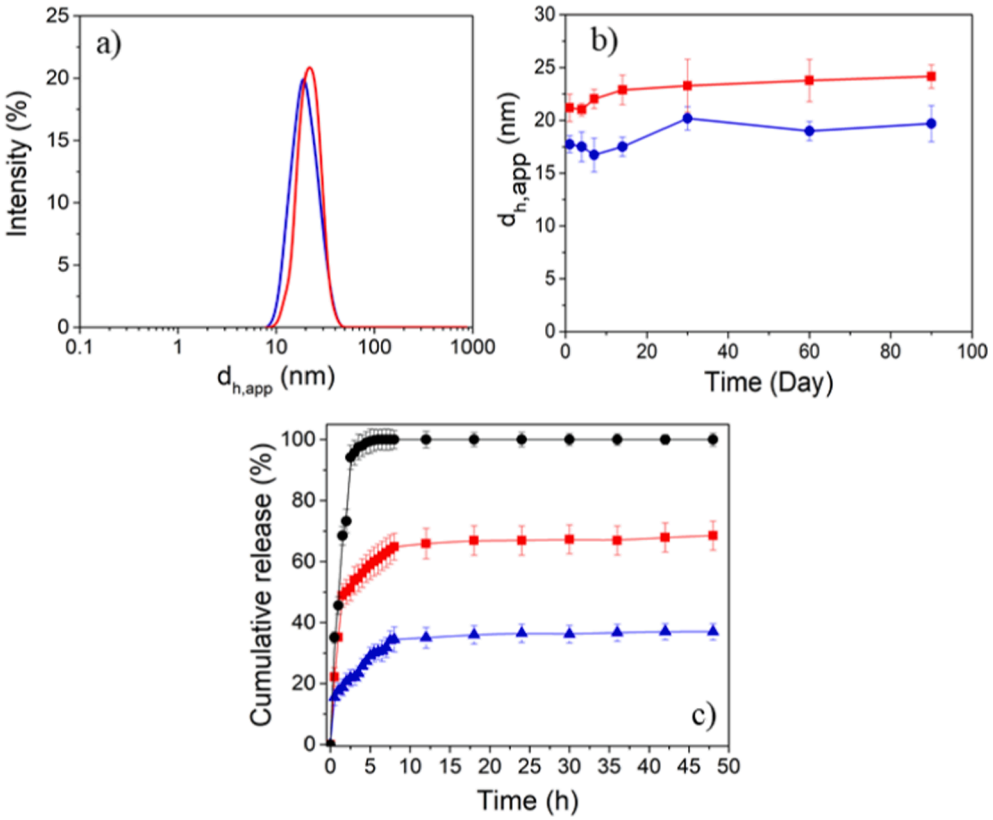

Fig. 1. A) hydrodynamic radii and b) zeta potential of both types of pht-loaded lignin (——, ■) and F127-stabilized (——, ●) nanomicelles. c) Release profiles of free PHT (●), and PHT-loaded lignin (■) and F127-stabilized (▲) nanomicelles in PBS at 37 °C and pH 7.4 for 48 h. Each value represents the mean ± S.D.

(F127 and lignin-based ones) was evaluated by the Alamar Blue assay [18,19]. Accordingly, fibroblasts (NIH/3T3) and PC12 cells were seeded in a 96 well plates (cell density 5×10^3 cells/well) containing RPMI culture medium, 10% (v/v) FBS, and 1% (v/v) penicillin–streptomycin and incubated in a humidified incubator at 37 °C with 5% CO_2 for 24 h. Then, different concentrations (5, 10, 20, 40, and 80 ng/mL) of free PHT, unloaded nanomicelles, and PHT-loaded nanomicelles (F127 and lignin-based ones) were added to each well (n = 5). Also, the culture medium containing cells without any added drug was used as a negative control. After 48 h, 10 μL of Alamar Blue (10% v/v) was added to each well, and the plates were incubated for 4 h at 37 °C and 5% CO_2. Next, light absorption was measured at 570 nm by means of an ELISA plate reader (BioTek, Bad Friedrichshall, and Germany), and the percentage of cell proliferation was calculated through the following equation:

$$Cellviability(\%) = \frac{(Testsampleabsorbance)}{(Controlsampleabsorbance)} \times 100 \quad (5)$$

2.7. Cell morphology evaluation

The morphology of PC12 and NIH/3T3 cells after administration of free PHT, unloaded and PHT-loaded nanomicelles (F127 and lignin-based) was analyzed by microscopy imaging. 8×10^3 cells/well were seeded in a 24 well plate containing RPMI 1640 culture medium, 10% (v/v) FBS and 1% (v/v) penicillin–streptomycin and incubated in a humidified incubator at 37 °C with 5% CO_2 for 24 h. Next, different concentrations (5, 10, 20, 40, and 80 ng/mL) of free PHT, unloaded and PHT-loaded nanomicelles (F127 and lignin-based ones) were added to each well (n = 5), and incubated again for 48 h. Changes in cell morphology were evaluated using an inverted light microscope (Olympus IX50; Olympus, Tokyo, Japan), at 10X magnification. The obtained images were taken by a digital camera.

2.8. Bacterial susceptibility testing

Blood culture vials with a volume of 25 or 50 mL from sterile sheep blood and containing sodium polyanetholesulfonate (SPS) as anticoagulant were kept at 2–8 ℃ (13,14). 5 mL of blood from culture medium were poured into sterile tubes with an equal volume in a class II biological safety cabinet with a standard sampler; then 1 mL of free PHT, F127/PHT-loaded, and lignin/ PHT-loaded nanomicelles was added, incubated for 24 h and checked for turbidity. The sterilized swab was then soaked in the sample and cultured in chocolate medium. This medium is a nonselective, enriched growth medium used for isolation of pathogenic bacteria essentially the same as blood agar except that during preparation the red blood cells are lysed by slowly heating to 80 °C,when added to molten agar base. As a result, the cell lysis releases intracellular nutrients such as hemoglobin, hemin ("X" factor), and the coenzyme nicotinamide adenine dinucleotide (NAD or "V" factor) into the agar used by bacteria.

Next, the tubes and the chocolate medium (pH 7.2) were incubated for 24 h and checked for microorganism growth. Analysis was repeated after the third, fifth and forteenth day of incubation.

2.9. Computer simulations

DFT calculations were conducted to acquire a molecular insight about the interactions of PHT with F127 and lignin inside the nanomicelles. For convenience, one F127 polymeric chain and the three main monomers that constitute the lignin structure, including coniferyl

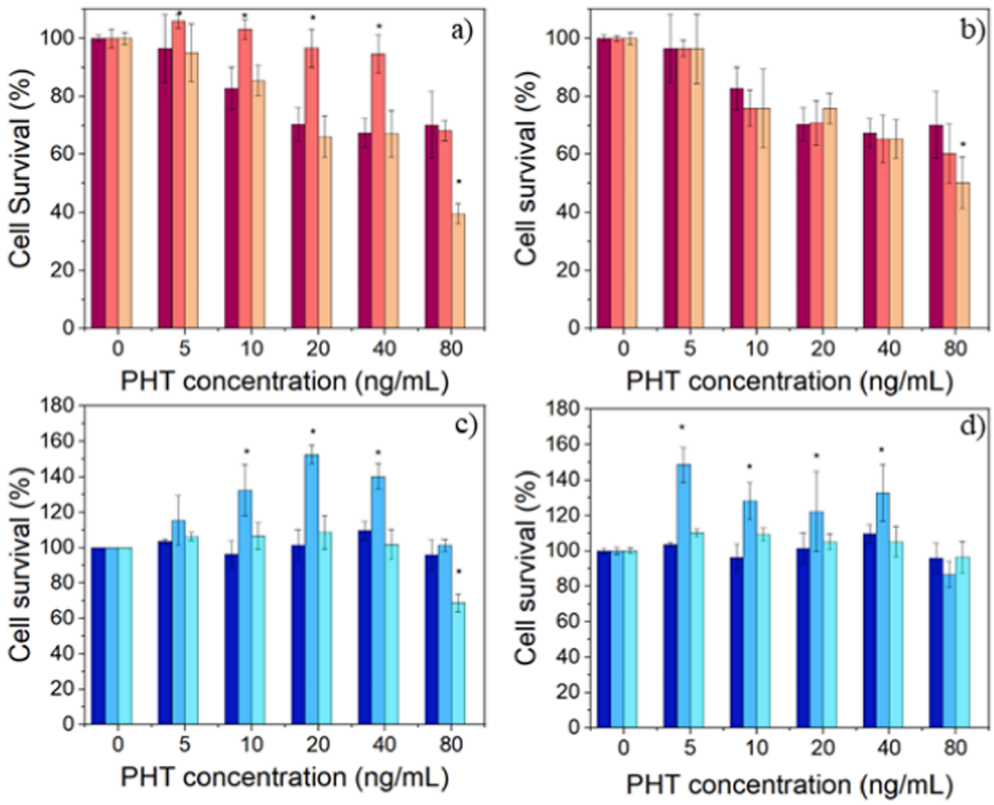

Fig. 2. Cytotoxicity of free PHT (,) PHT-loaded lignin stabilized (,) and F127-stabilized (,) nanomicelles after 48 h incubation by using the Alamar Blue assay: PHT-loaded a) lignin- and b) F127-stabilized nanomicelles in PC12 cells; and PHT-loaded c) lignin- and d) F127-stabilized nanomicelles in NIH/3T3 cells, (* $P < 0.05$). (For interpretation of the references to color in this figure legend, the reader is referred to the web version of this article.)

alcohol (CA), paracoumaryl alcohol (PCA) and sinapyl alcohol (SA), were chosen for the calculations. Gaussian09 program package using the B3LYP theoretical level by 6-31G(d) basis set was selected to optimize the geometry of monomers and solved the formed complexes [19]. AIM2000 was used to perform the electron charge density analysis at the B3LYP/6-31G(d) theoretical level [20,21]. The NBO program in Gaussian09 was used to perform a population analysis of the optimized structures and obtained resulting wave functions [20]. The interaction energy (ΔE) of binary complexes was calculated as follows:

$$\Delta E = E_{complex} - (E_{monomer1} + E_{monomer2}) \quad (6)$$

where $E_{complex}$ represents the total energy of the complex through interactions between PHT and the two polymers, while $E_{monomer1}$ and $E_{monomer2}$ denote the total energy of the optimized PHT and polymeric monomer, respectively. As an indicator of the strength of intermolecular HB interactions, binding energy (-ΔE) was used to evaluate the strength of interactions between PHT and two surfactants.

2.10. Statistical analysis

All of the results were stated in mean SD (mean standard deviation). Statistical analysis was done using SPSS 22.0. ANOVA analysis followed by Tuckey's Post Hoc test was used to compare the outcomes of the different groups. In this study, P-value < 0.05 was considered as statistically significant.

3. Results

3.1. Characterization of PHT-loaded surfactant-based nanomicelles

Two polymers acting as additional stabilizers were chosen in this study to be part of the ME-based nanomicelles composition to relate their different structures with their potential entrapment efficiency ability. F127 is a linear triblock copolymer with two lateral poly (ethylene oxide) blocks and a poly(oxypropylene) central one whereas lignin is a natural organic polymer formed by the polymerization of phenolic compounds, mainly of lipophilic character. F127 is a flexible polymer while lignin is more rigid and do not rotate. Nanomicelle formation was achieved by the oil-in-water ME technique using sodium caprylate as emulsifier and the mentioned polymers as droplet stabilizers. DLS data confirmed that PHT-loaded surfactant-based nanomicelles containing F127 and lignin have hydrodynamic diameters of ca. 16 ± 1 and 22 ± 2 nm, (see Fig. 1**a**) and surface charge of ca. −19.8 ± 2.3 and −20.5 ± 1.7 mV, respectively. On the other hand, Fig. 1**b** depicts the suitable colloidal stability of both types of nanomicelles, as confirmed by the absence of significant size changes upon storage for up to ca. 3 months in aqueous solution at 4 °C.

3.2. Drug encapsulation efficiency of PHT-loaded nanomicelles

According to the obtained experimental data, the EE% in F127/PHT-loaded and lignin/PHT-loaded nanomicelles was calculated to be 96.7 ± 1.5% and 68.2 ± 3.5%, respectively, both much higher than the EE% for ME-based nanomicelles in the absence of the polymeric stabilizers (ca. 35.2 ± 4.5%). The higher EE% of PHT-loaded, F127-stabilized nanomicelles is probably favored by the shorter and more flexible monomers of the copolymer which favor a better compaction within the micelle core, thus, enhancing its stabilization [20].

3.3. Drug release from PHT-loaded nanomicelles

The PHT release profile of free PHT, and from both types of PHT-loaded nanomicelles (F127/PHT-loaded and lignin/PHT-loaded ones) is shown in Fig. 1**c,** calculated by the accumulative PHT release from the

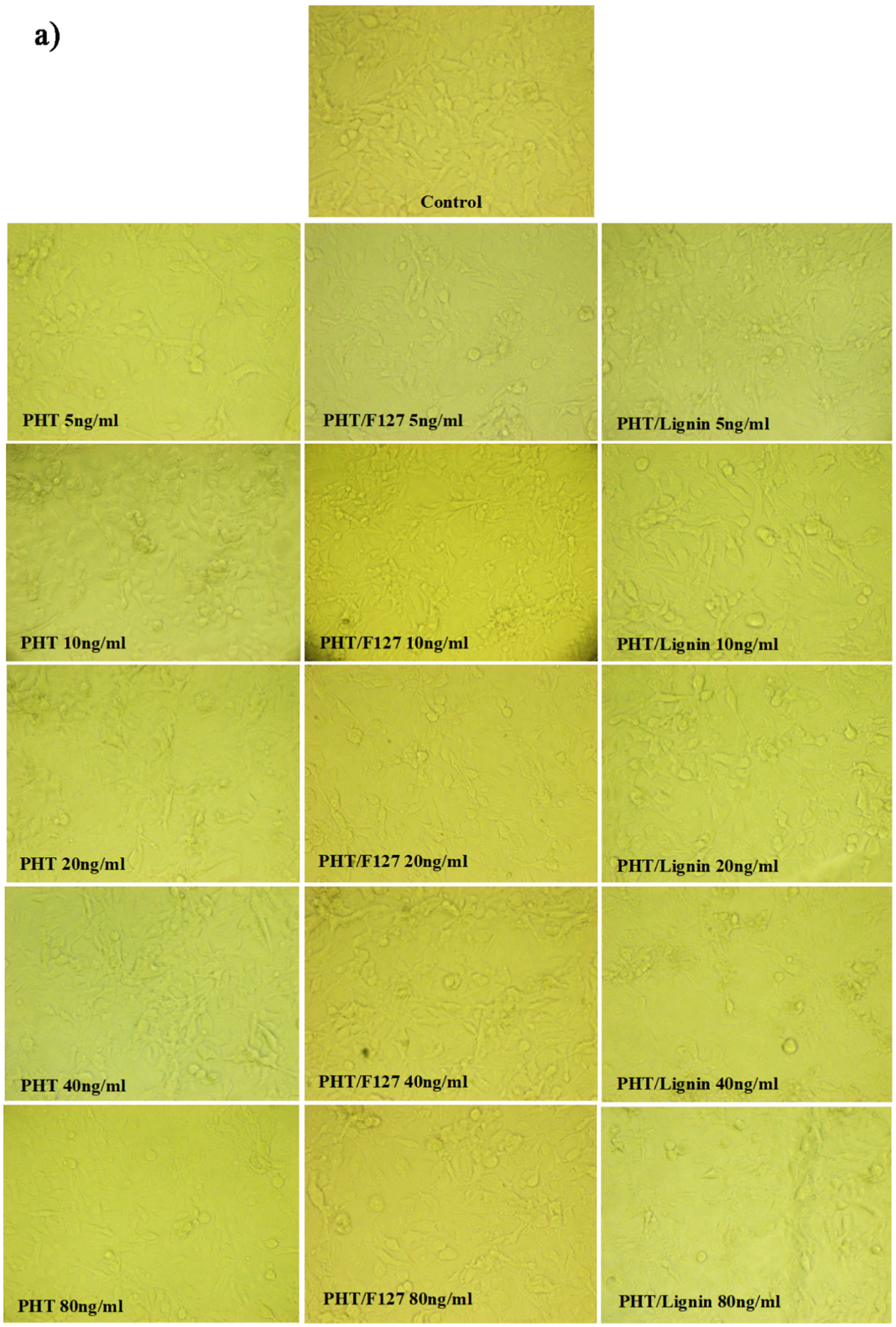

Fig. 3. Optical microscopy images of a) free PH, and PHT-loaded, lignin-stabilized and PHT-loaded, F127-stabilized nanomicelles to PC12 cells, and b) to NIHT3 ones after 48 h of incubation. Magnification: 20X in all images. The bar corresponds to 50 μm.

dialysis experiments. The release profile of free PHT profile showed that ca. 100% of the drug was released just after 4 h of incubation. Meanwhile, PHT released from F127 and lignin-stabilized nanomicelles showed a slower release kinetics. For PHT-loaded, F127-based nanomicelles there exists an initial burst phase within the first hour of incubation, in which up to ca. 18% of the drug was released and then, it progressively leveled off to reach ca. 39% of total drug after 48 h of incubation. For PHT-loaded, lignin-stabilized nanomicelles a similar

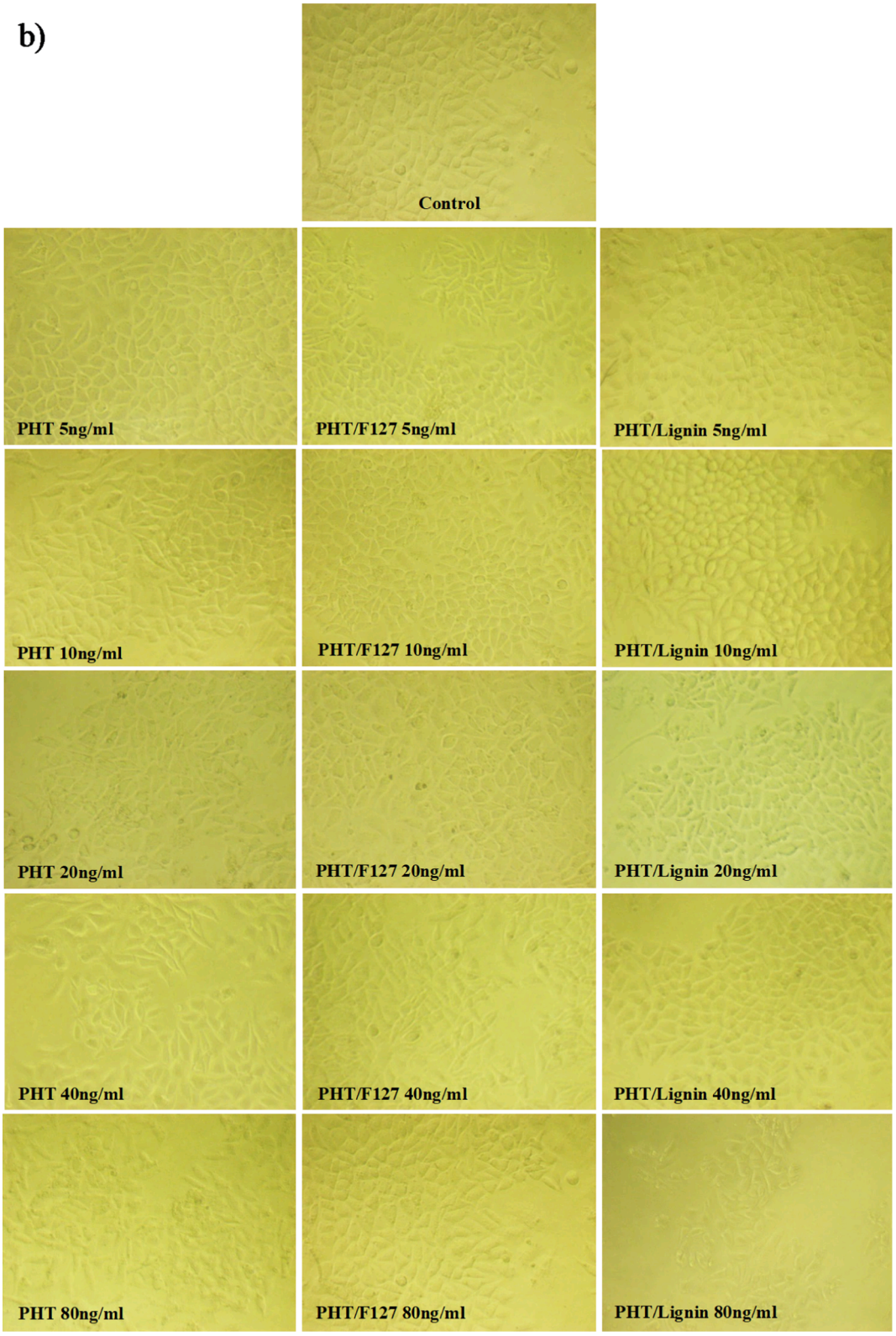

Fig. 3. (*continued*).

profile is observed, but up to ca. 41% of the bioactive cargo was released during the burst phase within the first hour and reaching ca. 68% after 48 h, respectively, probably as a result of a weaker, more porous micelle corona consequence of a worst accommodation of this biopolymer within the core-corona interface.

3.4. Cytotoxicity of PHT-loaded nanomicelles

Different concentrations of free drug and PHT-loaded nanomicelles stabilized with both F127 and lignin were used to evaluate the cytotoxicity of the drug *in vitro* using NIH/3T3 fibroblasts and PC12 cells. The embryonic mouse fibroblast cell line PC12 is a model of mature

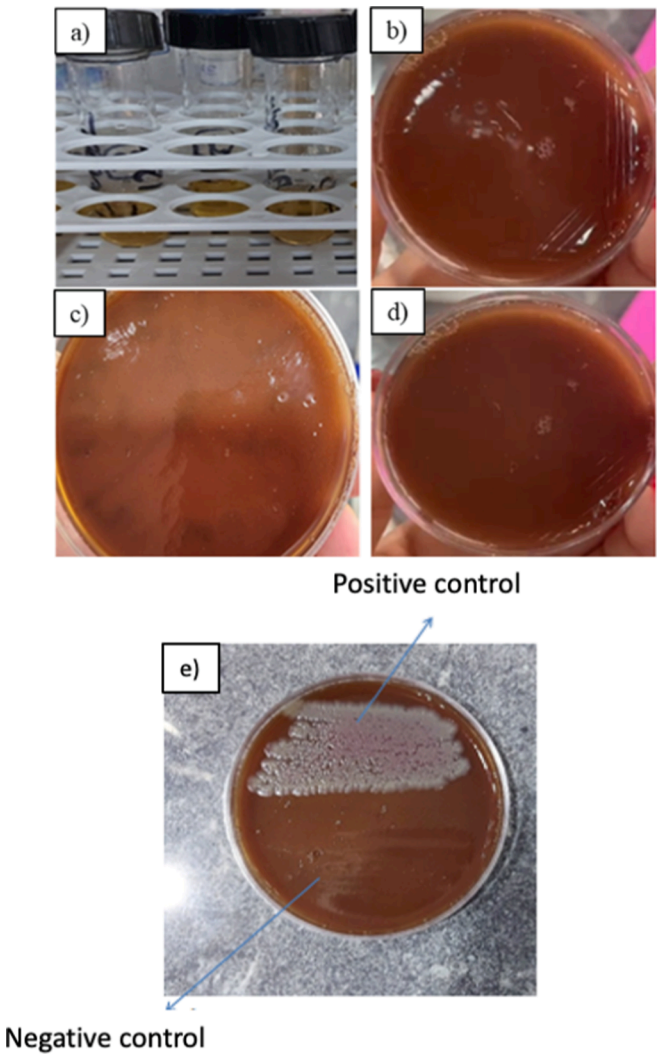

Fig. 4. A) blood tubes and blood culture in chocolate medium of b) free pht, c) pht-loaded, f-127-stabilized and d) pht-loaded, lignin-stabilized nanomicelles; e) positive and negative controls.

neuronal cell line that secretes catecholamines, dopamine, and norepinephrine and also present ion channels and neurotransmitter receptors, [23] whilst the NIH/3T3 embryonic mouse fibroblast cell line does not. The latter cell line is widely used in the development of drugs, cosmetics, etc as test cell line to analyze the cytotoxicity of (nano)materials and formulations as a result of their great sensitivity. Fig. 2**a-d** shows a toxic dose dependent behaviour on treated PC12 cells which is not observed for NIH/3T3 ones, and which should corroborate the effective chemo-effect of PHT in the target cell line while perfectly maintaining the viability on NIH/3T3 cells, that is, the vehicles are also cytocompatible. In this regard, the exposure of cells to concentrations larger than 40 ng/mL of both free and encapsulated PHT into F127 and lignin-stabilized nanomicelles caused a significant reduction in the proliferation of PC12 cells if compared to cell fibroblasts, being this decrease more important for the encapsulated cargo. It was also possible to observe that for PC12 cells a slightly higher cytotoxic effect was found for the PHT-loaded, lignin stabilized nanomicelles compared to F127-stabilized ones which can be attributed to the faster release pattern previously observed.

3.5. Cell morphological changes

Plasma membrane blebbing, cytoplasmic vacuolization, cell shrinkage, and chromatin condensation appear as important morphological cell changes related to cell apoptosis, leading to cell death. According to Fig. 3, by increasing the drug concentration from 5 to 40 ng/mL for both types of PHT-loaded nanomicelles, cell morphologies were observed to be preserved after administration of the nanoformulations in both PC12 and NIH/3T3 cells.

However, at a larger concentration of 80 ng/mL for PHT-loaded, lignin-stabilized nanomicelles a clear reduction in the number of visualized PC12 cells and an increasing view of rounded NIH/3T3 ones might be related to the development of cell toxic effects, being more important for the former cell type since as cells would detach from the plate indicative of cell death.

3.6. Assessment of the sterility of PHT-loaded nanomicelles

Localized or systemic infections can cause microorganisms to enter the blood stream but fortunately in most cases, bacteria are rapidly absorbed/detected/entrapped by the immune system [17]. Blood culture is a laboratory test to check the presence of bacteria or fungi in blood and is used to detect the presence of infection or if the manufacturing process of a formulation has been performed under suitable, sterile conditions [22]. Blood culture test consist of a culture media that favors a fast growth of those pathogens when present even at very low concentration, and it allows to identify if infection is occurring (within 24 h) and the type of germs present (within 48 h). The blood culture assay was used to check that the production methodology of the PHT-loaded nanomicelles is suitable to ensure sterile conditions for prospective application into the clinics and as a first step to intended GMP-compliant manufacturing. Blood culture for brain–heart infusion that contains beef or pig heart as well as calf brain, a source of amino acids (often either digested gelatin or other animal tissue), salt, disodium phosphate as a buffer, and glucose as a source of sugar was used. Data after 24 h of incubation showed that free PHT as control and both types of PHT-loaded nanomicelles at a concentration of 40 ng/mL do not promote bacterial growth (Fig. 4**a**) in agreement with the absence of sample turbidity. Data at longer incubation times (hours or days) showed also the absence of any pathogen in the Petri dishes, which confirmed that both nanoformulations maintained their sterile-like conditions and avoiding the growth and proliferation of existing potential pathogens in the blood samples used (Fig. 4**b-d**), probably as a consequence of some antimicrobial effect of PHT and some derivatives, as previously reported [24,25].

3.7. Computational analysis

DFT calculations were performed to investigate the bonding interactions between PHT and F127 and lignin monomeric chains as well as evaluating the interaction energy of resulting F127/PHT and lignin/PHT binary complexes to get further knowledge about the configuration and assembly of both polymers inside the nanomicelles. The interaction of PHT with F127 chains (denoted as F-PHT (1) for the poly(oxyethylene oxide) and F-PHT (2) for the poly(propylene oxide), respectively, and the three monomers of lignin (denoted as PCA for p-coumaryl alcohol, CA for coniferyl alcohol, and SA for sinapyl alcohol, respectively) were first geometrically optimized at the B3LYP theoretical level by the 6-31G (d) basis set in Gaussian09 software. Plots of the molecular electrostatic potential (MEP) maps of F127 and PHT showed electron-rich positions at O_{16}, O_{18}, O_{19} and O_{20} in F127 and at O_{28} and O_{29} in PHT, respectively (see Fig. 5).

Also, these maps showed that electron-rich positions are located at O_1, O_2, and O_3 atoms for CA monomer, O_1 and O_2 atoms for PCA monomer, and O_1, O_2, O_3, and O_4 atoms for SA monomer, respectively. We focused on these positions because they were prone to hydrogen bonding (HB) interactions with PHT, and all the intended binary complexes were developed on this basis. All these complexes were then optimized at the B3LYP/6-31G(d) level and their binding energy values

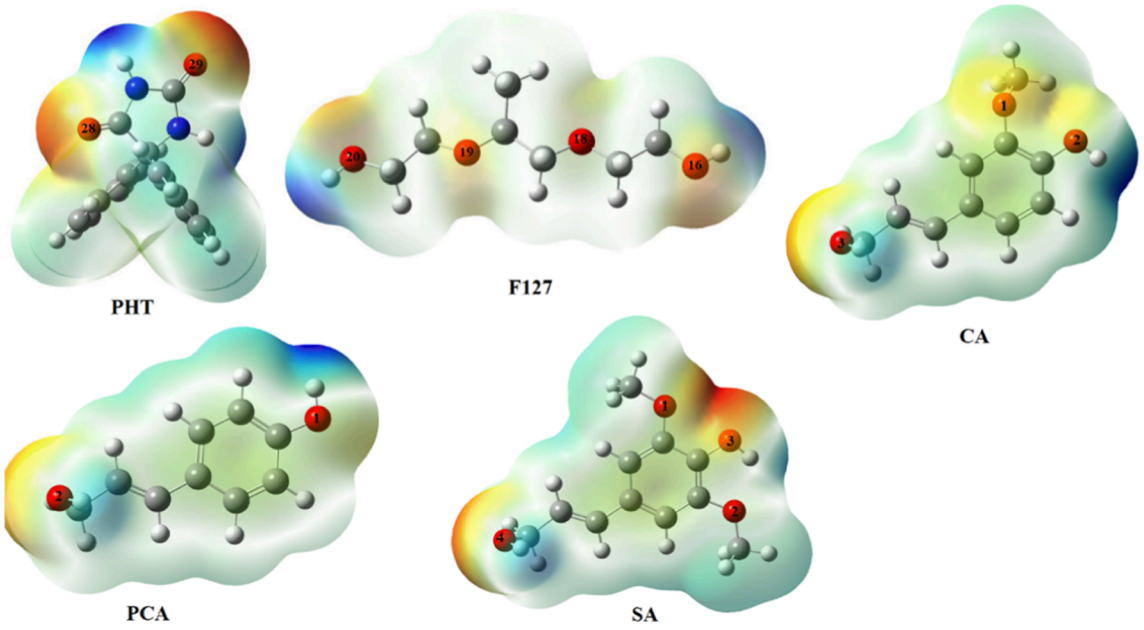

Fig. 5. MEP maps of PHT, F127, CA, PCA and SA.

obtained. Due to the large number of complexes, only the most stable ones with the highest binding energy were selected for further analysis. Fig. 6 depicts the optimized structures of the formed complexes as well as their binding energy values. The binding energies of F-PHT (1) and F-PHT (2) complexes were 12.64 and 11.74 kcal/mol, respectively. As seen, F-PHT (1) was more stable than F-PHT (2). Depending on the orientation of F127 and PHT relative to each other after optimization, (O_{20}-H_{21}…O_{29}) and (N_{31}-H_{48}…O_{20}) interactions exist for the F-PHT (1) complex giving rise to a six-membered ring; conversely, there exist (O_{16}-H_{17}…O_{28}) and (N_{31}-H_{48}…O_{16}) interactions for the F-PHT (2) complex but also leading to a similar ring structure. The binding energies of CA-PHT, PCA-PHT and SA-PHT complexes were 13.87, 12.62 and 11.69 kcal/mol, respectively. As shown, the most stable complex was related to the interaction between PHT with CA monomer of lignin. Given the orientation of PHT and these monomers, HB interactions between (O_2-H_{24}…O_{29}) and (N_3-H_{20}…O_2) in CA-PHT complex, (O_1-H_{20}…O_{29}) and (N_4-H_{21}…O_1) in PCA-PHT complex, and (O_4-H_{29}…O_{29}) and (N_3-H_{20}…O_4) in SA-PHT complex are observed, leading to the formation of six-membered rings in these complexes. The H…O bond length for the mentioned HB interactions is shown in Table 1. It is worth mentioning that the H_{24}…O_{29} bond length (1.807 Å) in the CA-PHT complex is shorter than for the others, and by increasing the HB strength the H…O bond length progressively declined.

On the other hand, AIM theory could help in evaluating the HB strength. The nature of binding interactions can be determined by analyzing the charge density (ρ) and its Laplacian ($\nabla^2\rho$) at the bond critical points (BCPs) between the two atoms that configured a hydrogen bond [5]. Table 1 shows the ρ_{BCP} and $\nabla^2\rho_{BCP}$ of HB of the formed binary complexes at the B3LYP/6-31G(d) theoretical level. The electronic kinetic energy density (G), the electronic potential energy density (V), and the total electronic energy density (H) were also computed in BCPs. The higher ρ_{BCP} for bond O_2-H_{24}…O_{29} of the CA-PHT complex confirmed a stronger HB, which is consistent with the finding suggesting H_{24}…O_{29} as the shortest and strongest bond. Data in Table 1 also showed that with a decrease in HB strength, ρ_{BCP} also decreases. Negative $\nabla^2\rho_{BCP}$ and H_{BCP} of all the complexes also confirmed strong HB interactions. Fig. 7 illustrates the molecular graphs of the complexes, BCPs, bond paths and HB interactions for all the complexes.

NBO analysis was also performed to additionally evaluate the HB strength in the complexes. The formation of HB suggests the transfer of a certain amount of electronic charge between the donor and receptor molecular orbitals in the complex and a rearrangement of electron density. The $E^{(2)}$ acceptor–donor stabilization energies were calculated for Lp(O) → σ^*_{OH} and Lp(O) → σ^*_{NH} interactions for all the complexes (Table 2). As observed, the profile of $E^{(2)}$ values was similar as those corresponding to the stability of the complexes, with PHT establishing the strongest interaction with CA monomer, following the sequence CA-PHT > PCA-PHT > F-PHT (1) > SA-PHT > F-PHT (1) complexes, and the O_{29} atom of PHT plays a key role in the formation of these bonds. Here, the O_{29} atom is the HB acceptor, and the electronic charge is transferred from a lone pair of O_{29} atom of PHT to the antibonding molecular orbital of the hydrogen donor monomers, thus playing an effective role in the stability of these complexes and in agreement with the observed slower drug release kinetics.

Thermodynamic properties, including Gibbs free energy (ΔG), enthalpy (ΔH) and entropy (ΔS) were assessed for F-PHT (1), F-PHT (2), CA-PHT, PCA-PHT and SA-PHT complexes (Table 3). The value of ΔG indicates a change in Gibbs free energy during the process of complex formation, and ΔG greater than 0 indicates that this complex formation is thermodynamically unfavorable. The observed high and negative TΔS is associated with the positive ΔG. Entropy then serves as the controlling factor in complex formation, and changes in entropy should exceed changes in enthalpy to yield a thermodynamic favorable process (TΔS > ΔH). Thus, CA-PHT and F-PHT (1) complexes with rather lower ΔG values were more stable than the other three ones. Also, negative ΔH values indicate that the interplay among the PHT, F127, CA, PCA and SA monomers is exothermic and enthalpically favourable.

4. Discussion

PHT is a classic antiepileptic drug that has multiple dose-dependent side effects. Drug encapsulation by the microemulsion technique favors drug loading and protection at the same time drug crystallization is avoided in the oily phase. Stabilization of the oil-in-water nanomicelles was successfully achieved with two different polymers, F127 and lignin, as additional stabilizers of the nanoformulations in the form of ca. 16–22 nm sized nanomicelles. Both nanosystems were shown to be successful nanocarriers for the entrapment of PHT. The obtained results confirmed the higher ability of F127-stabilized nanomicelles to encapsulate PHT (ca. 97% EE) in comparison with lignin-stabilized ones (ca.

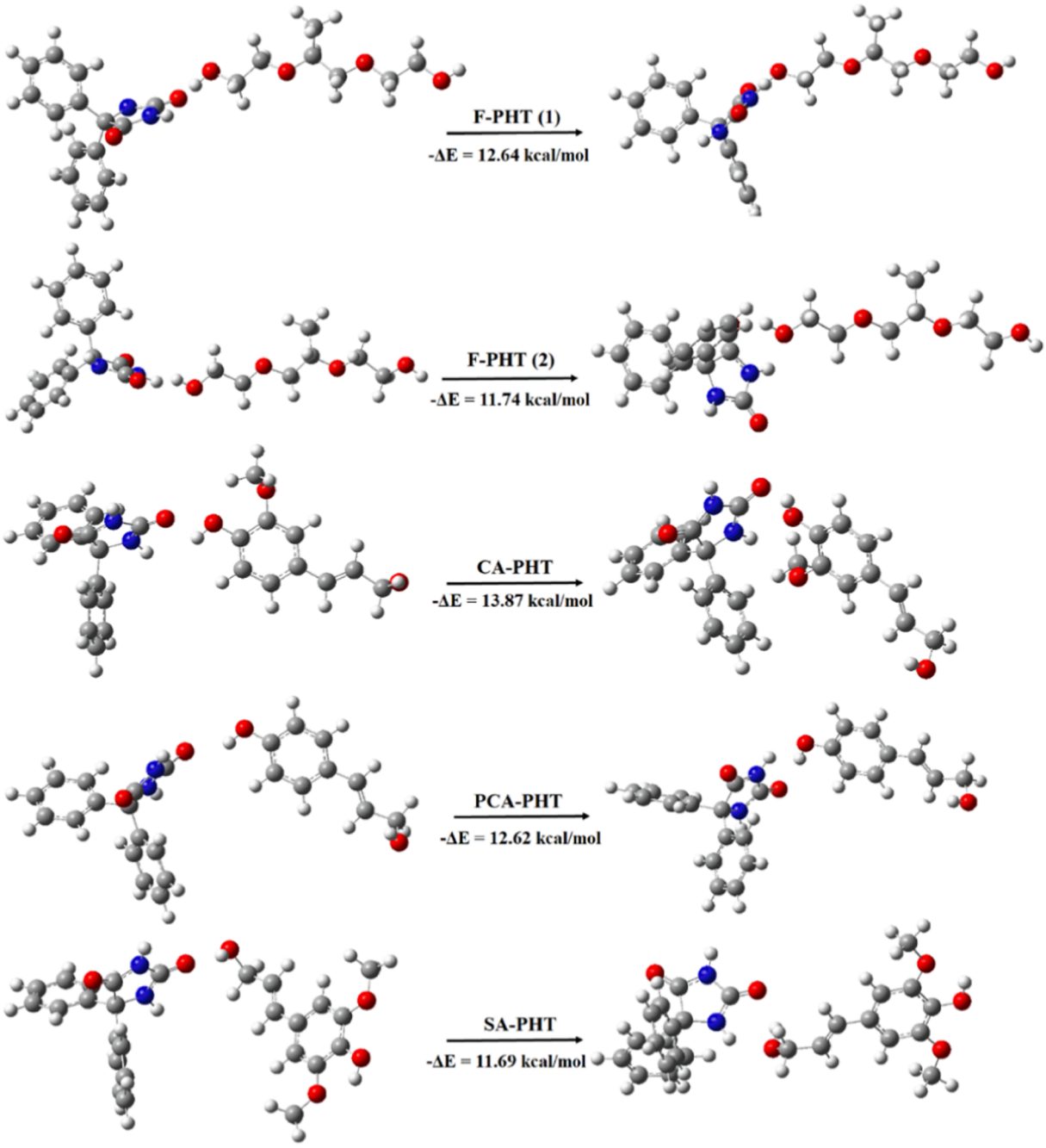

Fig. 6. Initial (left) and optimized (right) structures of the formed complexes, and binding energy values (in kcal/mol).

Table 1
Hydrogen bond lengths (Å) and topological parameters of F127/PHT and lignin/PHT complexes (au).

Complex	HB	Bond length	$\nabla^2\rho_{BCP}$	G_{BCP}	V_{BCP}	H_{BCP}
F-PHT (1)	O_{20}-H_{21}…O_{29}	1.914	−0.022508	0.023859	−0.025209	−0.001350
	N_{31}-H_{48}…O_{20}	1.974	−0.020521	0.021777	−0.023033	−0.001256
F-PHT (2)	O_{16}-H_{17}…O_{28}	1.945	−0.020947	0.022237	−0.023528	−0.001291
	N_{31}-H_{48}…O_{16}	1.994	−0.019819	0.020927	−0.022036	−0.001109
CA-PHT	O_2-H_{24}…O_{29}	1.807	−0.028488	0.030071	−0.031654	−0.001583
	N_3-H_{20}…O_2	2.074	−0.017561	0.018026	−0.018490	−0.000464
PCA-PHT	O_1-H_{20}…O_{29}	1.817	−0.027850	0.029323	−0.030796	−0.001473
	N_4-H_{21}…O_1	2.131	−0.015365	0.015512	−0.015658	−0.000146
SA-PHT	O_4-H_{29} …O_{29}	1.968	−0.020069	0.021279	−0.022490	−0.001211
	N_3-H_{20}…O_4	1.982	−0.020132	0.021337	−0.022542	−0.001205

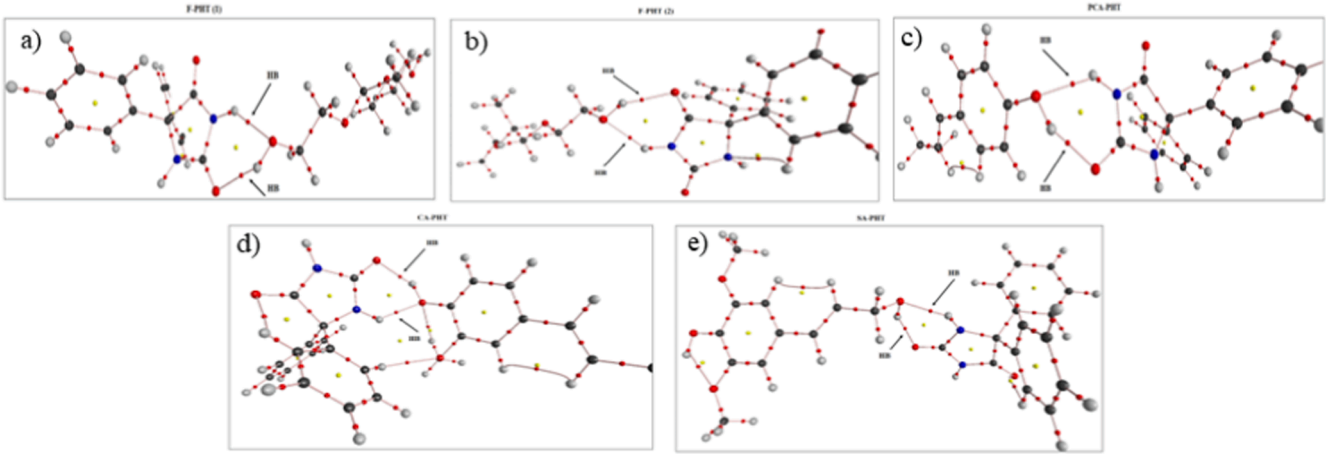

Fig. 7. Molecular graphs of the studied complexes: a) F-PHT-(1), b) F-PHT-(2), c) CA-PHT, d) PCA-PHT, e) SA-PHT. Color code: Red globes denote BCPs whilst yellow globes denote ring critical points (RCPs). (For interpretation of the references to color in this figure legend, the reader is referred to the web version of this article.)

Table 2
Charge transfer energies of F127/PHT and lignin/PHT complexes at B3LYP/6-31G(d) level (in kcal/mol).

Sample		Charge transfer energies
F-PHT (1)	$Lp(O_{29}) \rightarrow \sigma^*O_{20}H_{21}$	13.73
	$Lp(O_{20}) \rightarrow \sigma^*N_{31}\text{-}H_{48}$	10.88
F-PHT (2)	$Lp(O_{28}) \rightarrow \sigma^*O_{16}H_{17}$	12.08
	$Lp(O_{16}) \rightarrow \sigma^*N_{31}\text{-}H_{48}$	10.08
CA-PHT	$Lp(O_{29}) \rightarrow \sigma^* O_2\text{-}H_{24}$	20.9
	$Lp(O_2) \rightarrow \sigma^*N_3\text{-}H_{20}$	6.39
PCA-PHT	$Lp(O_{29}) \rightarrow \sigma^*O_1\text{-}H_{20}$	20.17
	$Lp(O_1) \rightarrow \sigma^*N_4\text{-}H_{21}$	5.49
SA-PHT	$Lp(O_{29}) \rightarrow \sigma^*O_4\text{-}H_{29}$	11.46
	$Lp(O_4) \rightarrow \sigma^*N_3\text{-}H_{20}$	10.98

Table 3
Thermodynamic parameters of F127/PHT and lignin/PHT complexes (in kcal/mol).

Complex	ΔG	ΔH	TΔS
F-PHT (1)	−1.098	−10.893	−9.794
F-PHT (2)	−0.267	−10.010	−9.741
CA-PHT	−1.551	−12.219	−10.667
PCA-PHT	−0.870	−10.947	−10.076
SA-PHT	−0.840	−10.032	−9.192

68% EE) as a consequence of the larger flexibility and strong amphiphilic character of the block copolymer. DFT simulations were performed to study the PHT interactions with the different polymeric monomers that composed the two polymers, being found multiple O rich regions that form multiple strong HBs (11–14 kcal/mol) that lead to a ring conformation. Negative free Gibbs energies were obtained for all the PHT-polymer complexes studied, indicating that PHT-polymer conjugation is a thermodynamically favored process (AG < 0). On the other hand, drug release profiles from both types of nanoformulations (F127- and lignin-stabilized) showed a much slower PHT release kinetics compared to free drug and reaching a stationary phase of accumulated drug release after 8 h of incubation with ca. 39 and 68% of the encapsulated cargo in solution. PHT release data *in vitro* then seem to corroborate the strong binding between PHT and polymeric monomers, since a complete drug release from the micelles cannot be achieved within the experimental time frame. Cell viability assays in PC12 cells, in which PHT can block Na + channels, exhibit a dose-dependent behaviour whereas in NIH/3T3 ones do not. In this regard, cell survival is reduced to 45% and 40% when F127- and lignin-stabilized nanomicelles are loaded with 80 ng/ml of PHT, respectively, while similar concentrations do not alter the viability of NIH/3T3 fibroblasts. In addition, PHT-loaded nanomicelles (either stabilized with F127 or lignin) have a positive impact on the growth of NIH/3T3 cells. Morphological alterations such as cell shrinkage, membrane damage, cytoplasmic vacuolization, and formation of apoptotic bodies were observed in PC12 cells exposed to PHT-loaded nanomicelles compared to NIH/3T3 cell ones, which confirmed PHT therapeutic efficacy. The obtained images also confirmed the absence of any toxic/adverse side effect of PHT-loaded micelles on NIH/3T3 cells, which maintain their morphology. In summary, both proposed nanoformulations loaded, protected and delivered PHT even when the formed micelles structure is different because of the lipophilic domains of the used polymers. Calculated binding energies agree with the obtained release data, leading to a potential therapeutic effect on the targeted cell line at a lower dose than commonly used (10–20 mg/kg) while preserving the viability on healthy cells, which corroborates the selectivity of the treatment. In addition, blood culture studies of PHT-loaded F127 and lignin-stabilized nanomicelles reveal the aseptic character of the production methodology of these nanoformulations which make it amenable for prospective use in clinic after determining the absence of pathogens after several days incubation.

5. Conclusions

The current experimental and theoretical findings shed light to exploit PHT-loaded F127 and lignin-stabilized nanomicelles for the efficient PHT entrapment, protection and controlled release. Polymeric stabilizers here used offer great potential to enhance therapeutic outcome of the developed nanoformulations by exploiting their physicochemical properties, as the aseptic conditions promoted by lignin-PHT loaded nanomicelles or the potentially favored BBB trespassing ability of F127-based ones. Both nanoformulations have nanometer size (ca. 16–22 nm) and negatively surface charge (ca. −20 mV) and achieved high PHT entrapment efficiencies ranging from ca. 70% for lignin-stabilized nanomicelles to ca. 95% for F127-based ones and sustained release patterns. Additional benefits related to drug entrapment would be the avoidance of drug crystallization inside the nanomicelle oily core and the reduction of undesired drug side effects upon administration. Simulation data provided information about the role played by hydrogen bonding in the stabilization of the drug inside the nanomicelle core, accounting for the high efficiency values achieved. In particular, it was clearly determined that an electron charge transition from a lone pair of atoms O_{29} (LpO) in PHT to the anti-bonding orbitals of O_{20}-H_{21} (σ*OH) in F127 and O_2-H_{24} (σ*OH) in lignin affects the stability of the

F127/PHT and lignin/PHT complexes, respectively. In addition, *in vitro* data showed that the bare developed nanocarrier was non-toxic to cells and the PHT-loaded nanomicelles induced toxicity in a dose-dependent manner selective for Na + channels present in PC12 cells, corroborated at concentrations as low as 80 ng/mL. Moreover, cell death mechanisms appear to be potentially related to an apoptotic pathway as deduced from the change in cell morphologies, which adopted spherical symmetries with a reduction in cell density. Based on the presented experimental data, both formulations offer great potential as anti-seizure treatment. Further research will be done to decipher all the treatment potential before translation to clinical practice.

Institutional review board statement

The *in vitro* part of the study protocol was approved by Mashhad University of Medical Sciences (Ethical code: 991620.).

CRediT authorship contribution statement

Nafiseh Jirofti: Investigation, Validation, Data curation, Methodology, Writing – original draft. **Mahdiyeh Poorsargol:** Investigation, Validation, Methodology, Writing – original draft. **Farkhonde Sarhaddi:** Conceptualization, Formal analysis, Writing – review & editing. **Afsaneh Jahani:** Investigation, Validation, Data curation, Methodology. **Jamileh Kadkhoda:** Investigation, Data curation, Methodology. **Fatemeh Kalalinia:** Resources, Methodology, Formal analysis, Writing – review & editing. **Abbas Rahdar:** Methodology, Writing – review & editing. **Adriana Cambón:** Validation, Formal analysis, Visualization, Writing – review & editing. **Pablo Taboada:** Formal analysis, Visualization, Writing – review & editing.

Declaration of Competing Interest

The authors declare that they have no known competing financial interests or personal relationships that could have appeared to influence the work reported in this paper.

Data availability

Data will be made available on request.

Acknowledgements

The authors would like to thank Dr. Maryam Abolhasani (Associate Professor of Pathology, Iran University of Medical Sciences). P.T. also thanks Agencia Estatal de Investigación (AEI) by project PID2019-109517RB-I00. ERDF funds are also acknowledged.

References

[1] J. Patocka, Q. Wu, E. Nepovimova, K. Kuca, Phenytoin–An anti-seizure drug: Overview of its chemistry, pharmacology and toxicology, Food Chem. Toxicol. 142 (2020), 111393, https://doi.org/10.1016/j.fct.2020.111393.
[2] A. Iorga, B. Z. Horowitz, Phenytoin Toxicity. StatPearls. StatPearls Publishing, Treasure Island (FL), USA. 2023. https://www.ncbi.nlm.nih.gov/books/NBK482444/.
[3] R.G. Ricarte, N.J. Van Zee, Z. Li, L.M. Johnson, T.P. Lodge, M.A. Hillmyer, Recent advances in understanding the micro-and nanoscale phenomena of amorphous solid dispersions, Mol. Pharm. 16 (2019) 4089–4103, https://doi.org/10.1021/acs.molpharmaceut.9b00601.
[4] A. Yousfan, N. Rubio, A.H. Natouf, A. Daher, N. Al-Kafry, K. Venner, H. Kafa, Preparation and characterisation of PHT-loaded chitosan lecithin nanoparticles for intranasal drug delivery to the brain, RSC Adv. 10 (2020) 28992–29009, https://doi.org/10.1039/D0RA04890A.
[5] H.K. Alajangi, M. Kaur, A. Sharma, S. Rana, S. Thakur, M. Chatterjee, N. Singla, P. K. Jaiswal, G. Singh, R.P. Barnwal, Blood–brain barrier: emerging trends on transport models and new-age strategies for therapeutics intervention against neurological disorders, Mol. Brain 15 (2022) 49, https://doi.org/10.1186/s13041-022-00937-4.
[6] X. Niu, J. Chen, J. Gao, Nanocarriers as a powerful vehicle to overcome blood-brain barrier in treating neurodegenerative diseases: Focus on recent advances, Asian J. Pharm. Sci. 14 (2019) 480–496, https://doi.org/10.1016/j.ajps.2018.09.005.
[7] L. Tang, Y. Feng, S. Gao, Q. Mu, C. Liu, Nanotherapeutics overcoming the blood-brain barrier for glioblastoma treatment, Front. Pharmacol. 12 (2021), 786700, https://doi.org/10.3389/fphar.2021.786700.
[8] A. Froelich, T. Osmałek, B. Jadach, V. Puri, B. Michniak-Kohn, Microemulsion-based media in nose-to-brain drug delivery, Pharmaceutics 13 (2021) 201, https://doi.org/10.3390/pharmaceutics13020201.
[9] S.P. Acharya, K. Pundarikakshudu, P. Upadhyay, P. Shelat, A. Lalwani, Development of phenytoin intranasal microemulsion for treatment of epilepsy, J. Pharm. Investig. 45 (2015) 375–384, https://doi.org/10.1007/s40005-015-0190-3.
[10] S. Lee, C.C. Teo, W. Tan, H. Lim, H.H. Lim, S.Y. Teo, Lipid microemulsion-based hydrogels for effective topical delivery of phenytoin, Int. J. Pharm. Pharm. Sci. 8 (2016) 240–246. https://doi.org/10.22159/ijpps.2016v8i11.13394.
[11] G.M. Peterson, S. McLean, S. Aldous, R.J. Von Witt, K.S. Millingen, Plasma protein binding of phenytoin in 100 epileptic patients, British J. Clin. Pharmacol. 14 (1982) 298–300, https://doi.org/10.1111/j.1365-2125.1982.tb01981.x.
[12] W. Löscher, H. Potschka, Drug resistance in brain diseases and the role of drug efflux transporters, Nature Rev. Neurosci. 6 (2005) 591–602, https://doi.org/10.1038/nrn1728.
[13] J. Liu, Y. He, J. Zhang, J. Li, X. Yu, Z. Cao, F. Meng, Y. Zhao, X. Wu, T. Shen, Z. Hong, Functionalized nanocarrier combined seizure-specific vector with P-glycoprotein modulation property for antiepileptic drug delivery, Biomaterials 74 (2016) 64–76, https://doi.org/10.1016/j.biomaterials.2015.09.041.
[14] A. Cambón, J. Brea, M.I. Loza, C. Alvarez-Lorenzo, A. Concheiro, S. Barbosa, P. Taboada, V. Mosquera, Cytocompatibility and P-glycoprotein inhibition of block copolymers: Structure-activity relationship, Mol. Pharm. 10 (2013) 3232–3241, https://doi.org/10.1021/mp4002848.
[15] A. Cambón, A. Rey-Rico, S. Barbosa, J.F.A. Soltero, S.G. Yeates, J. Brea, M.I. Loza, C. Alvarez-Lorenzo, A. Concheiro, P. Taboada, V. Mosquera, Poly(styrene oxide)-poly(ethylene oxide) block copolymers: From "classical" chemotherapeutic nanocarriers to active cell-response inducers, J. Control. Release 167 (2013) 68–75, https://doi.org/10.1016/j.jconrel.2013.01.010.
[16] A. Alzagameem, S.E. Klein, M. Bergs, X.T. Do, I. Korte, S. Dohlen, C. Hüwe, J. Kreyenschmidt, B. Kamm, M. Larkins, M. Schulze, Antimicrobial activity of lignin and lignin-derived cellulose and chitosan composites against selected pathogenic and spoilage microorganisms, Polymers 11 (2019) 670, https://doi.org/10.3390/polym11040670.
[17] W. Yang, E. Fortunati, F. Bertoglio, J.S. Owczarek, G. Bruni, M. Kozanecki, J. M. Kenny, L. Torre, L. Visai, D. Puglia, Polyvinyl alcohol/chitosan hydrogels with enhanced antioxidant and antibacterial properties induced by lignin nanoparticles, Carbohydrate Polym. 181 (2018) 275–284, https://doi.org/10.1016/j.carbpol.2017.10.084.
[18] A. Rahdar, P. Hasanein, M. Bilal, H. Beyzaei, G.Z. Kyzas, Quercetin-loaded F127 nanomicelles: Antioxidant activity and protection against renal injury induced by gentamicin in rats, Life Sci. 276 (2021), 119420, https://doi.org/10.1016/j.lfs.2021.119420.
[19] A. Rahdar, M.R. Hajinezhad, S. Sargazi, M. Barani, P. Karimi, B. Velasco, P. Taboada, S. Pandey, Z. Bameri, S. Zarei, Pluronic F127/carfilzomib-based nanomicelles as promising nanocarriers: Synthesis, characterization, biological, and in silico evaluations, J. Mol. Liq. 346 (2022), 118271, https://doi.org/10.1016/j.molliq.2021.118271.
[20] N. Jirofti, M. Golandi, J. Movaffagh, F.S. Ahmadi, F. Kalalinia, Improvement of the wound-healing process by curcumin-loaded chitosan/collagen blend electrospun nanofibers: in vitro and in vivo studies, ACS Biomater. Sci. Eng. 7 (2021) 3886–3897, https://doi.org/10.1021/acsbiomaterials.1c00131.
[21] F. Kalalinia, Z. Taherzadeh, N. Jirofti, N. Amiri, N. Foroghinia, M. Beheshti, B.S. F. Bazzaz, M. Hashemi, A. Shahroodi, E. Pishavar, Evaluation of wound healing efficiency of vancomycin-loaded electrospun chitosan/poly ethylene oxide nanofibers in full thickness wound model of rat, Int. J. Biol. Macromol. 177 (2021) 100–110, https://doi.org/10.1016/j.ijbiomac.2021.01.209.
[22] S. Sargazi, M.R. Hajinezhad, M. Barani, M. Mukhtar, A. Rahdar, F. Baino, P. Karimi, S. Pandey, F127/cisplatin microemulsions: in vitro, in vivo and computational studies, Appl. Sci. 11 (2021) 3006, https://doi.org/10.3390/app11073006.
[23] B. Wiatrak, A. Kubis-Kubiak, A. Piwowar, E. Barg, PC12 cell line: cell types, coating of culture vessels, differentiation and other culture conditions, Cells 9 (2020) 958, https://doi.org/10.3390/cells9040958.
[24] O.M. Ali, H.H. Amer, A.A. Mosaad, A.-A.-H. Abdel-Rahman, Synthesis and antimicrobial activity of new phenytoin derivatives and their acyclic nucleoside analogs, Chem. Heterocyclic Comp. 48 (2012) 1043–1049, https://doi.org/10.1007/s10593-012-1097-9.
[25] N. Esiobu, N. Hoosein, An assessment of the in vitro antimicrobial effects of two antiepileptic drugs – sodium valproate and phenytoin, Antonie van Leeuwenhoek 83 (2003) 63–68, https://doi.org/10.1023/A:1022992224594.